

Electronic Supplementary information for

Iron and Nitrogen Co-doped CoSe₂ Nanosheet Arrays for Robust Electrocatalytic Water Oxidation

Di Li^a, Yingying Xing^a, Changjian Zhou^a, Yikai Lu^b, Shengjie Xu^b, Xiangli Shi^a, Deli Jiang*, and Weidong Shi^{b,*}

^a Institute for Energy Research, Jiangsu University, Zhenjiang 212013, China

^b School of Chemistry and Chemical Engineering, Jiangsu University, Zhenjiang 212013, China

Corresponding author: Deli Jiang; Weidong Shi

E-mail address:

dlj@ujs.edu.cn (D. Jiang)

swd1978@ujs.edu.cn (W. Shi)

Fig. S1 SEM and TEM images of precursor.....	3
Fig. S2 FT-IR spectra of the as-obtained samples	4
Fig. S3 SEM images of CoSe ₂ -based catalysts.....	5
Fig. S4 N ₂ adsorption-desorption isotherms for catalysts.	6
Fig. S5 STEM-EDX spectrum of the Fe-N-CoSe ₂	7
Fig. S6 LSV of Fe-CoSe ₂ catalyst with different Fe content.....	8
Fig. S7 Cyclic voltammogram (CV) curves of the catalysts with different scan rates.....	9
Fig. S8 CVs of samples in PBS solution (pH = 7) at a scan rate of 50 mV s ⁻¹	11
Fig. S9 Turnover frequency (TOF) curves of the catalysts.	12
Fig. S10 A digital photograph showing the continuous generation of O ₂ bubbles on the Fe-N-CoSe ₂ catalyst.	14
Fig. S11 Collect the generated O ₂ by the drainage method and record the data every 5 minutes...15	15
Fig. S12 TEM images of Fe-N-CoSe ₂ electrocatalyst after long-term OER durability test.....	16
Fig. S13 XRD of Fe-N-CoSe ₂ electrocatalyst after long-term OER durability test.....	17
Fig. S14 XPS analysis of Fe-N-CoSe ₂ electrocatalyst after long term OER stability test.	18
Table S1 The physical properties of all as-prepared materials.	19
Table S2 Composition of CoSe ₂ -based catalysts.	20
Table S3 Comparison of OER performance of Fe-N-CoSe ₂ catalyst with the most efficient non-noble metal catalysts recently reported in 1 M KOH.	21
References	22

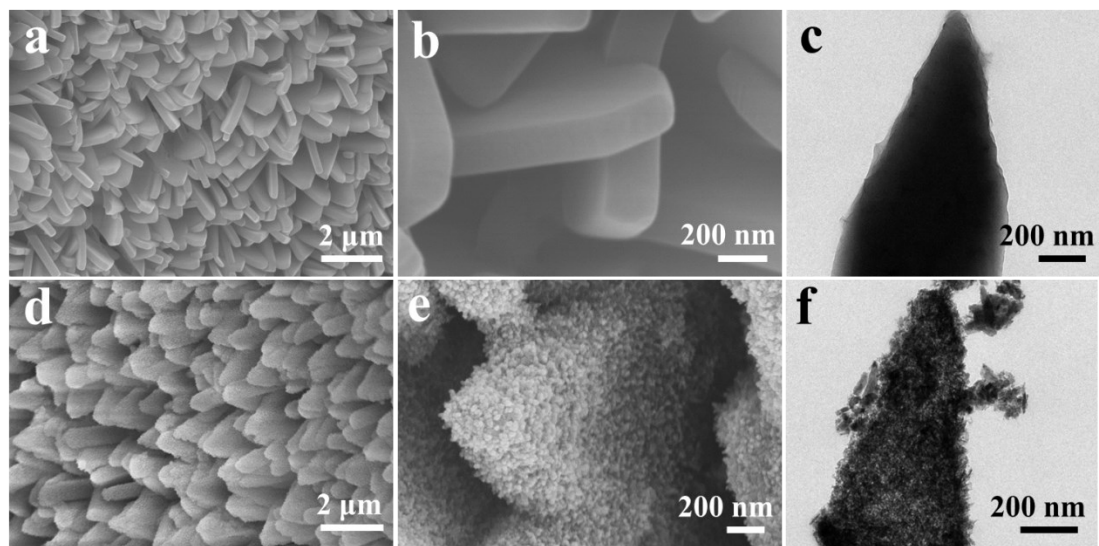


Fig. S1 SEM and TEM images of precursor: (a-c) Co-MOF, (d-f) CoFe-PBA.

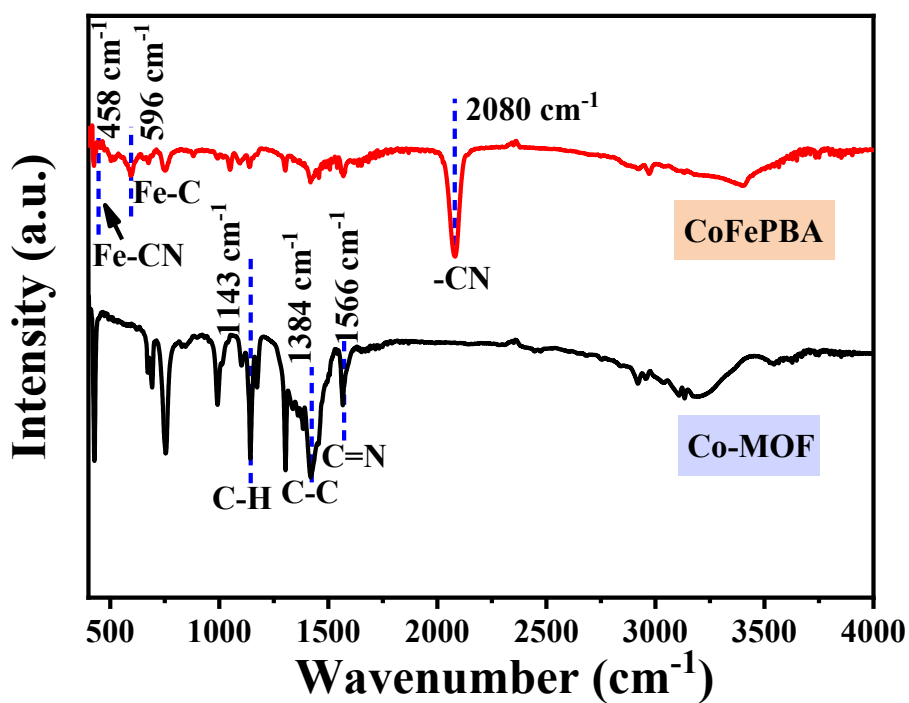


Fig. S2 FT-IR spectra of the as-obtained Co-MOF and CoFe-PBA.

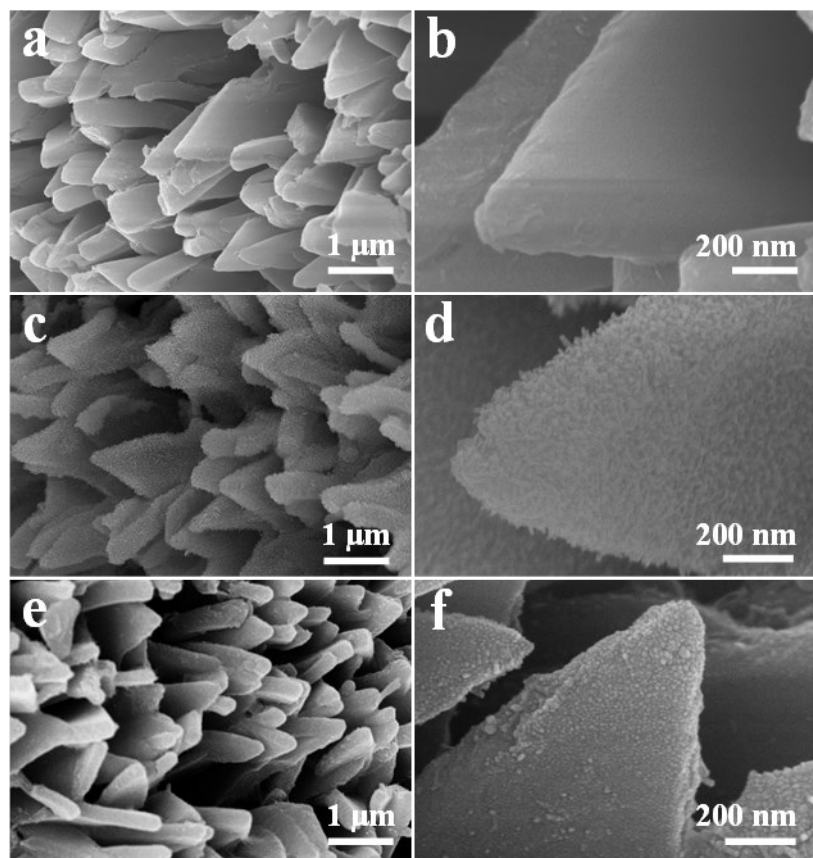


Fig. S3 SEM images of CoSe₂-based catalysts: (a, b) CoSe₂, (c, d) Fe-CoSe₂, and (e, f) N-CoSe₂.

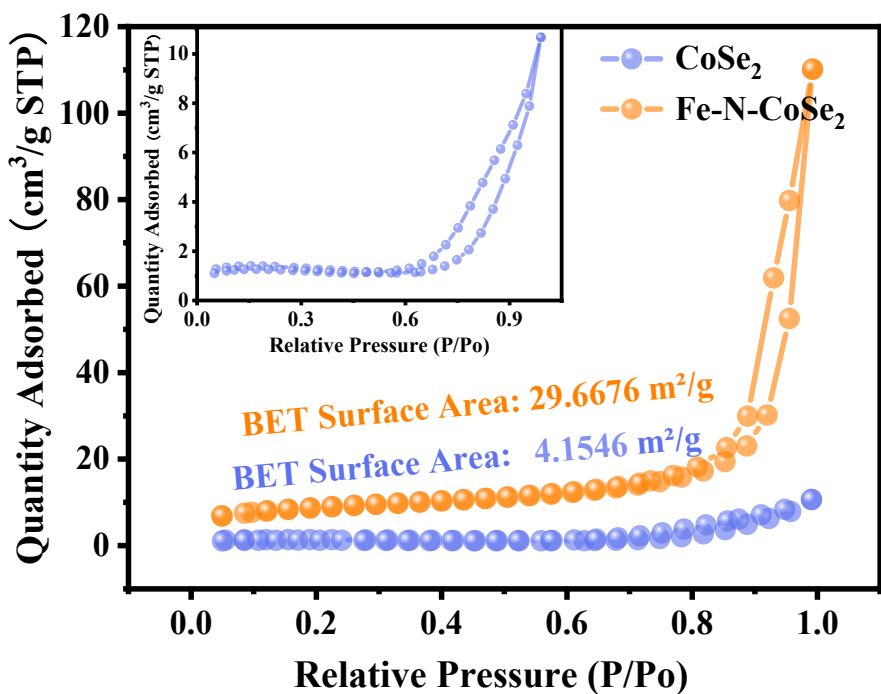


Fig. S4 N₂ adsorption-desorption isotherms for CoSe₂ and Fe-N-CoSe₂ catalyst, respectively.

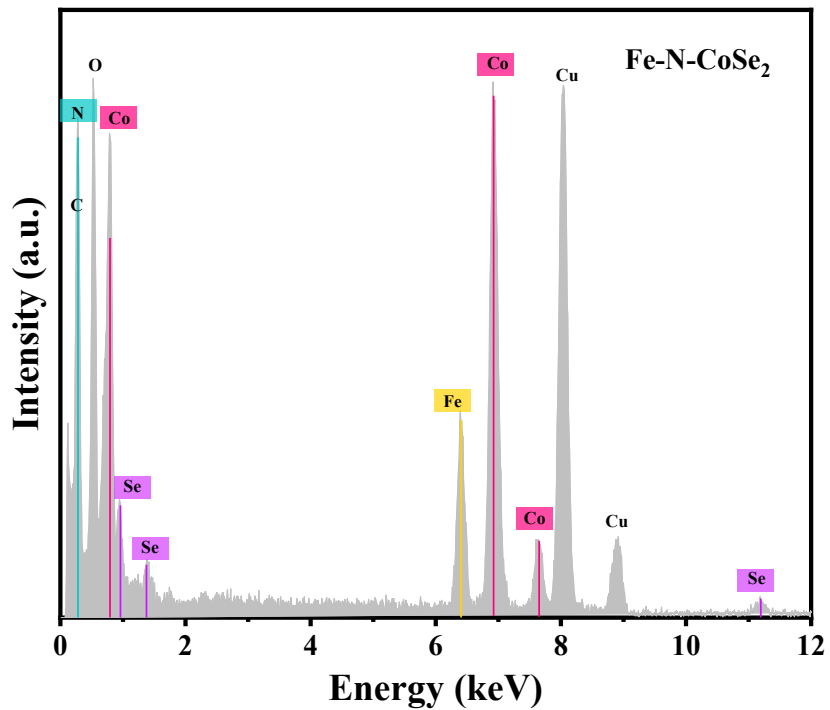


Fig. S5 STEM-EDX spectrum of the Fe-N-CoSe₂. The peaks of Cu are originated from the copper grid.

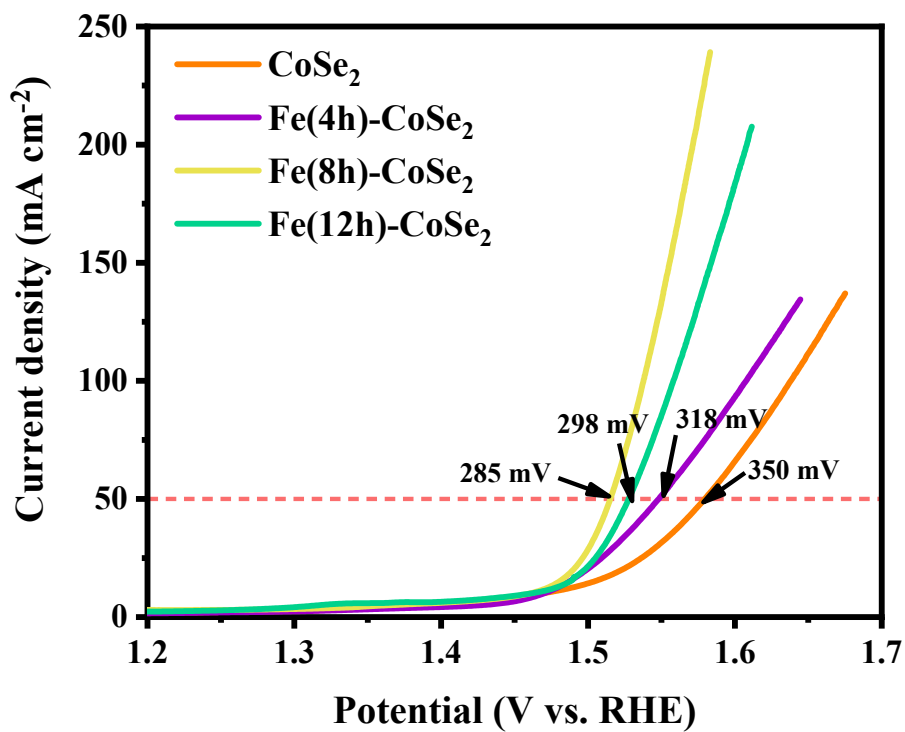


Fig. S6 LSV of $\text{Fe}\text{-CoSe}_2$ catalyst with different Fe content for OER in 1 M KOH solution.

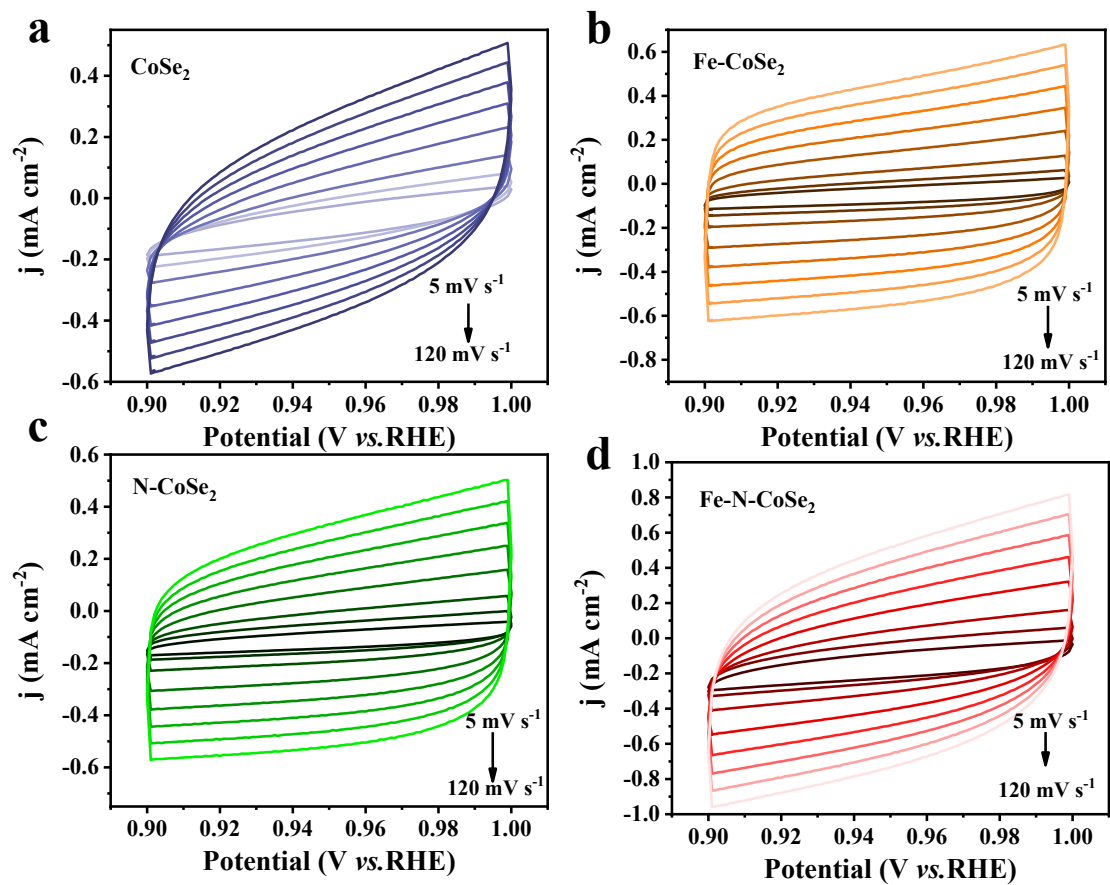


Fig. S7 Cyclic voltammogram (CV) curves of the catalyst. (a) CoSe₂, (b) Fe-CoSe₂ (c) N-CoSe₂ and (d) Fe-N-CoSe₂ in 1 M KOH between 0.9 V and 1.0 V vs. RHE.

TOF calculation process:

By using the previous reported method to calculate the TOF of CoSe₂, Fe-CoSe₂, N-CoSe₂, Fe-N-CoSe₂, CV measurements with potential window from 0.6 V to 1.2 V vs. RHE were carried out in phosphate buffered saline (PBS, pH = 7), where we assumed that no oxygen evolution reaction together with electrochemical corrosion of our samples happened.

The TOF could be calculated with the following equation:

$$\text{TOF} = I/Q$$

Where I (A) is the current of the polarization curve, we obtained it from the LSVs measurements. Voltammetric charges (Q) is calculated by the following equation:

$$Q = 4Fn$$

Where F is Faraday constant (96480 C mol⁻¹), n is the number of active sites. In the experiment, the voltammometry curve is obtained by CVs measurements with phosphate buffer (pH = 7) at a scan rate of 50 mV s⁻¹. When the number of voltammetric (Q) is obtained after deduction of the blank value.

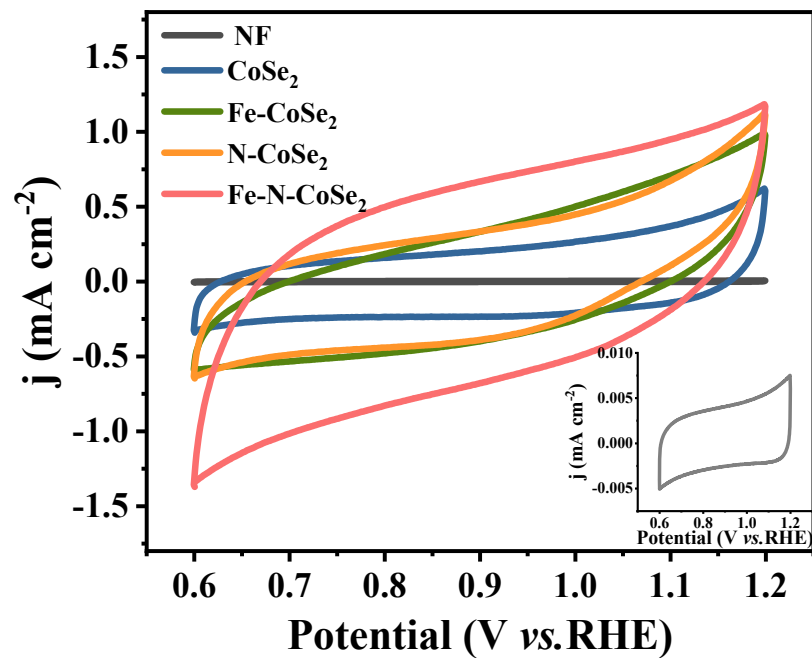


Fig. S8 CVs of sample NF, CoSe₂, Fe-CoSe₂, N-CoSe₂ and Fe-N-CoSe₂ in PBS solution (pH = 7) at a scan rate of 50 mV s⁻¹.

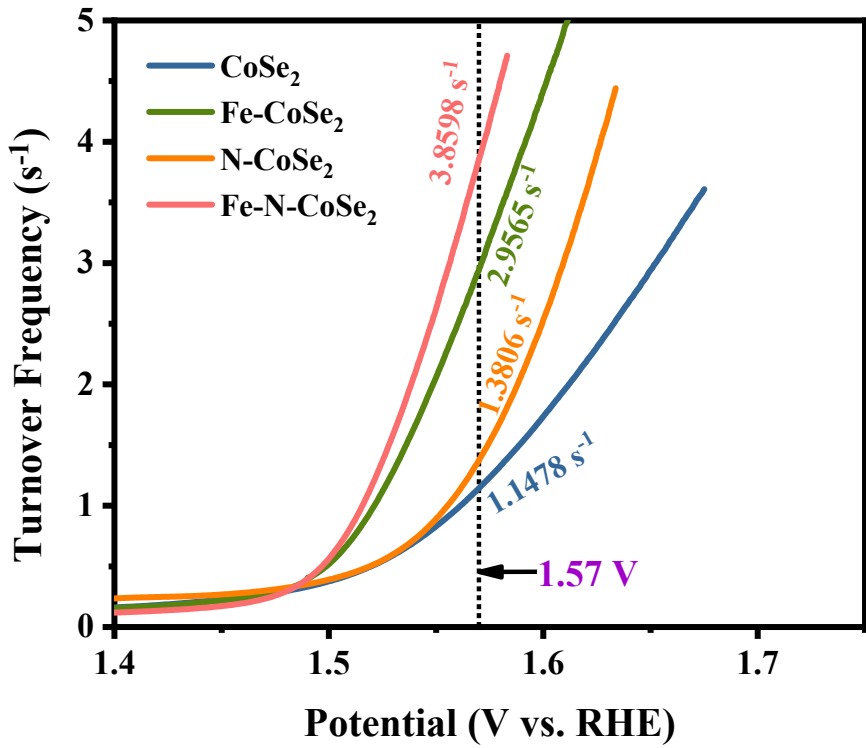


Fig. S9 Turnover frequency (TOF) curves of the CoSe_2 , $\text{Fe}-\text{CoSe}_2$, $\text{N}-\text{CoSe}_2$ and $\text{Fe}-\text{N}-\text{CoSe}_2$ catalysts.

Faraday efficiency calculation:

To investigate the Faradaic efficiency for O₂ evolution for Fe-N-CoSe₂, O₂ gas was collected by a water drainage method. The corresponding theoretical value was determined by assuming the 100% conversion of electric current according to the Faraday law during the electrolysis. The data in **Fig.s S10** and **S11** show the correlation between the molar amount of O₂ gas produced and the time. The Faraday efficiency during OER was calculated based on the ratio of the amount of O₂ evolved to the theoretical value.

The theoretical number of moles of the gas calculated by the charge passed through the electrode.

$$n_g(\text{theoretical}) = \frac{Q}{zF}$$

Where n_g is the number of moles of the gas produced, Q is the charge passed through the electrodes, z means z mole electrons per mole O₂ (z = 4), F is Faraday constant (96485 C mol⁻¹). Thus, Faradaic efficiency can be determined by the following equation:

$$FE\% = \frac{n_g(\text{experimental})}{n_g(\text{theoretical})} \times 100\%$$

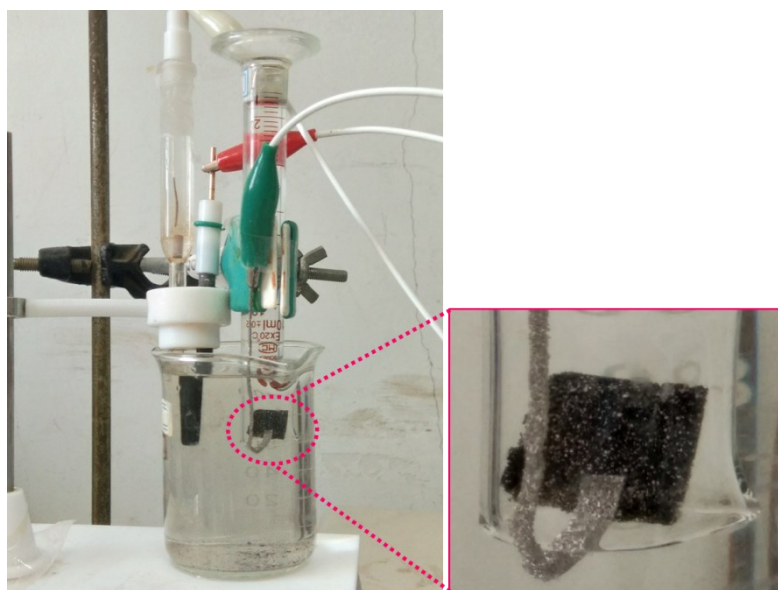


Fig. S10 A digital photograph showing the continuous generation of O₂ bubbles on the Fe-N-CoSe₂ catalyst.

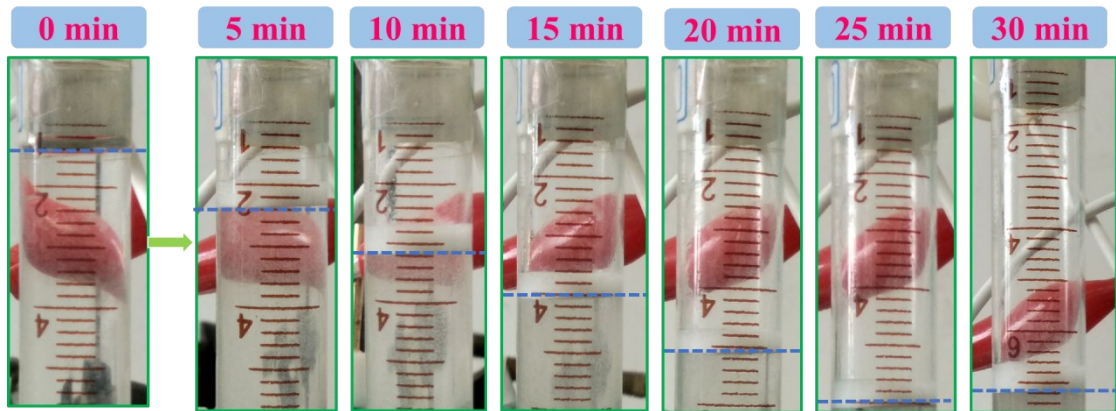


Fig. S11 Collect the generated O₂ by the drainage method and record the data every 5 minutes.

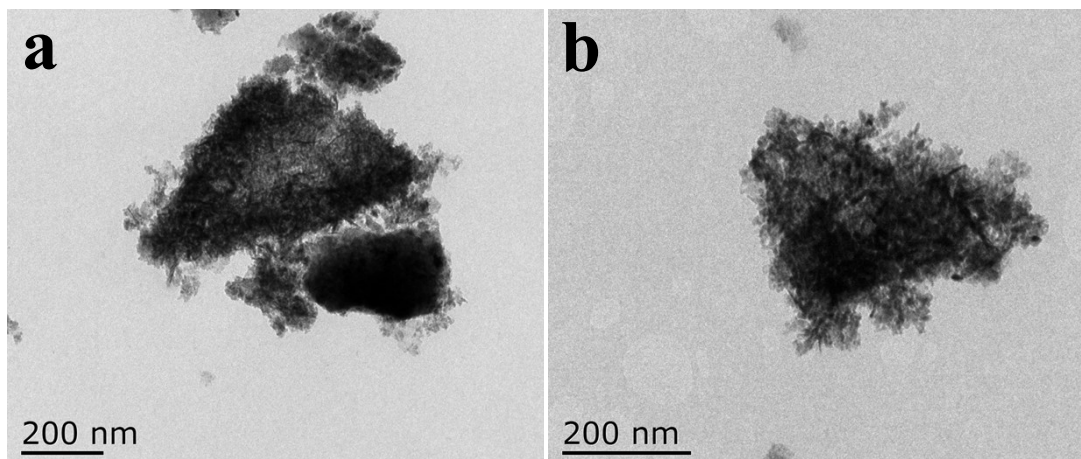


Fig. S12 TEM images of Fe-N-CoSe₂ electrocatalyst after long-term OER durability test.

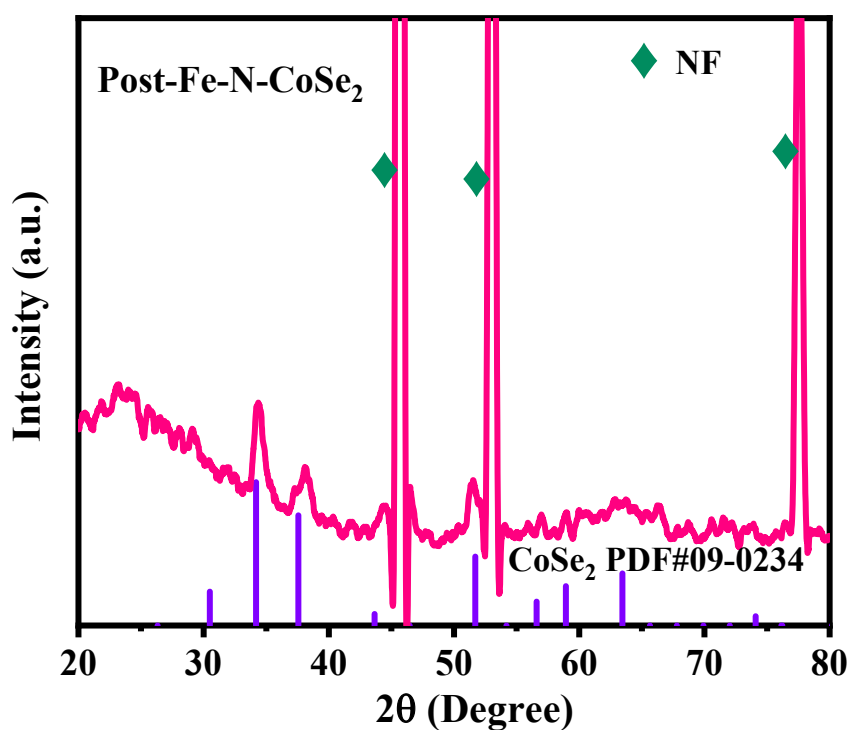


Fig. S13 XRD of Fe-N-CoSe₂ electrocatalyst after long-term OER durability test.

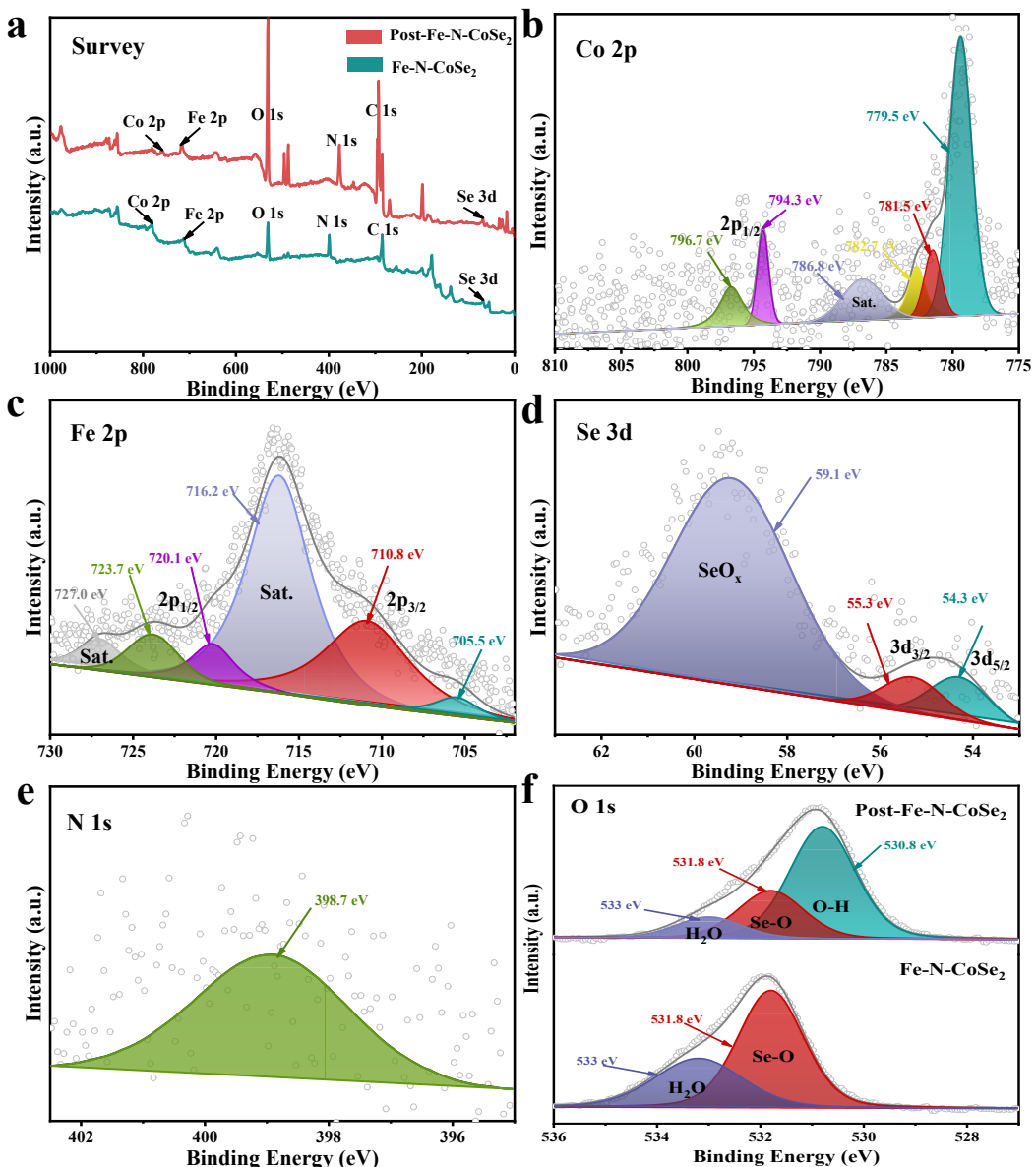


Fig. S14 XPS analysis of Fe-N-CoSe₂ electrocatalyst recorded after long term OER stability test: (a) Survey of the Fe-N-CoSe₂ and Post-Fe-N-CoSe₂, (b) Co 2p, (c) Fe 2p, (d) Se 3d, (e) N 1s and (f) O 1s of the Fe-N-CoSe₂ and Post Fe-N-CoSe₂.

Table S1 The physical properties of all as-prepared materials.

Catalysts	Nanosheet thickness (nm)	2θ of (210) plane (°)
CoMOF	160	-
CoFePBA	553	-
CoSe ₂	345	33.84
Fe-CoSe ₂	414	33.82
N-CoSe ₂	283	34.26
Fe-N-CoSe ₂	463	33.96

Table S2 Composition of CoSe₂-based catalysts.

Catalyst	XPS							ICP	EA
	Co/%	Se/%	Fe/%	N/%	Se/Co	Fe/Co%	N/Se%	Fe/Co%	N/Se%
CoSe ₂	33.61	64.21	/	/	1.91			/	/
Fe-N-CoSe ₂	25.88	46.04	10.04	19.01	1.78	38.8	41.3	38.3	43.61

Table S3 Comparison of OER performance of Fe-N-CoSe₂ catalyst with the most efficient non-noble metal catalysts recently reported in 1 M KOH.

Catalysts	Overpotential (mV)	Tafel slope (mV dec ⁻¹)	Electrolyte	Reference work
Fe-N-CoSe ₂	270@50 mA cm ⁻²	63.7	1M KOH	This work
S:CoP@NF	270@10mA cm ⁻² 330@50mA cm ⁻²	62.7	1M KOH	1
Fe _x Co _{2-x} P/NF	273@50 mA cm ⁻²	55	1M KOH	2
Co ₂ P@Co/N-C/GC	320@10 mA cm ⁻²	48.8	1M KOH	3
Ni ₂ P-CoP/GC	320@10 mA cm ⁻²	69	1M KOH	4
Co _{0.85} Se@NC	320@10 mA cm ⁻²	75	1M KOH	5
NiSe/NF	270@20 mA cm ⁻²	64	1M KOH	6
Ni _{0.88} Co _{1.22} Se ₄	340@10 mA cm ⁻²	78	1M KOH	7
Ni-Co-P HNB	270@10 mA cm ⁻²	76	1M KOH	8
NiCoPO/NC	300@10 mA cm ⁻²	94	1M KOH	9
N-CNTs@NiS ₂ /Fe ₇ S ₈	330@50 mA cm ⁻²	51.49	1M KOH	10
Fe-UNT	270@10 mA cm ⁻²	36.3	1M KOH	11
NiCo-LDH@FeOOH/CF	224@10 mA cm ⁻²	38	1M KOH	12
CoFePO	274.5@10 mA cm ⁻²	51.7	1M KOH	13
NiCoFeP	273@10 mA cm ⁻²	35	1M KOH	14
Fe ₅ Co ₄ Ni ₂₀ Se ₃₆ B _x	279.8@10 mA cm ⁻²	59.5	1M KOH	15

References

- [1] M. A. R. Anjum, M. S. Okyay, M. Kim, M. H. Lee, N. Park, J. S. Lee, Bifunctional sulfur-doped cobalt phosphide electrocatalyst outperforms all-noble-metal electrocatalysts in alkaline electrolyzer for overall water splitting, *Nano Energy*, 2018, **53**, 286.
- [2] T. I. Singh, G. Rajeshkhanna, S. B. Singh, T. Kshetri, N. H. Kim, J. H. Lee, Metal-organic framework-derived Fe/Co-based bifunctional electrode for H₂ production through water and urea electrolysis, *ChemSusChem*, 2019, **12**, 1–15.
- [3] C. Zhu, S. Fu, B. Z. Xu, J. Song, Q. Shi, M. H. Engelhard, X. Li, S. P. Beckman, J. Sun, D. Du, Y. Lin, Sugar blowing-induced porous cobalt phosphide/nitrogen-doped carbon nanostructures with enhanced electrochemical oxidation performance toward water and other small molecules, *Small*, 2017, **13**, 1700796.
- [4] X. Liang, B. Zheng, L. Chen, J. Zhang, Z. Zhuang, B. Chen, MOF-derived formation of Ni₂P-CoP bimetallic phosphides with strong interfacial effect towards electrocatalytic water splitting, *ACS Appl. Mater. Interfaces*, 2017, **9**, 23222–23229.
- [5] T. Meng, J. W. Qin, S. G. Wang, D. Zhao, B. G. Mao, M. H. Cao, In situ coupling of Co_{0.85}Se and N-doped carbon via one-step selenization of metal-organic frameworks as a trifunctional catalyst for overall water splitting and Zn-air batteries, *J. Mater. Chem. A*, 2017, **5**, 7001–7014.
- [6] C. Tang, N. Y. Cheng, Z. H. Pu, W. Xing, X. P. Sun, NiSe nanowire film supported on nickel foam: an efficient and stable 3D bifunctional electrode for full water splitting, *Angew. Chem. Int. Ed.*, 2015, **54**, 9351–9355.

- [7] D. V. Shinde, L. D. Trizio, Z. Y. Dang, M. Prato, R. Gaspari, L. Manna, Hollow and porous nickel cobalt perselenide nanostructured microparticles for enhanced electrocatalytic oxygen evolution, *Chem. Mater.*, 2017, **29**, 7032–7041.
- [8] E. L. Hu, Y. F. Feng, J. W. Nai, D. Zhao, Y. Hu, X. W. Lou, Construction of hierarchical Ni-Co-P hollow nanobricks with oriented nanosheets for efficient overall water splitting, *Energy Environ. Sci.*, 2018, **11**, 872–880.
- [9] C. S. Wang, W. B. Chen, D. Yuan, S. S. Qian, D. D. Cai, J. T. Jiang, S. Q. Zhang, Tailoring the nanostructure and electronic configuration of metal phosphides for efficient electrocatalytic oxygen evolution reactions, *Nano Energy*, 2020, **69**, 104453.
- [10] J. Y. Wang, W. T. Liu, X. P. Li, T. Ouyang, Z. Q. Liu, Strong hydrophilicity $\text{NiS}_2/\text{Fe}_7\text{S}_8$ heterojunctions encapsulated in N-doped carbon nanotubes for enhanced oxygen evolution reaction, *Chem. Commun.*, 2020, **56**, 1489–1492.
- [11] G. Q. Shen, R. R. Zhang, L. Pan, F. Hou, Y. J. Zhao, Z. Y. Shen, W. B. Mi, C. X. Shi, Q. F. Wang, X. W. Zhang, J. J. Zou, Regulating spin state of Fe(III) by atomically anchoring on ultrathin titanium dioxide for efficient oxygen evolution electrocatalysis, *Angew. Chem. Int. Ed.*, 2020, **59**, 2313–2317.
- [12] X. T. Han, Y. Y. Niu, C. Yu, Z. B. Liu, H. W. Huang, H. L. Huang, S. F. Li, W. Guo, X. Y. Tan, J. S. Qiu, Ultrafast construction of interfacial sites by wet chemical etching to enhance electrocatalytic oxygen evolution, *Nano Energy*, 2020, **69**, 104367.
- [13] J. J. Duan, S. Chen, A. Vasileff, S. Z. Qiao, Anion and cation modulation in metal

compounds for bifunctional overall water splitting, *ACS Nano*, 2016, **10**, 8738–8745.

[14] Y. N. Guo, J. Tang, Z. L. Wang, Y. Sugahara, Y. Yamauchi, Hollow porous heterometallic phosphide nanocubes for enhanced electrochemical water splitting, *Small*, 2018, **14**, 1802442.

[15] Y. P. Zuo, D. W. Rao, S. N. Ma, T. T. Li, Y. H. Tsang, S. Kment, Y. Chai, Valence engineering via dual-cation and boron doping in pyrite selenide for highly Efficient oxygen evolution, *ACS Nano*, 2019, **13**, 11469–11476.